Chinese Chemical Letters 32 (2021) 3015–3018

Contents lists available at ScienceDirect

Chinese Chemical Letters

journal homepage: www.elsevier.com/locate/cclet

Communication

Mechanism and selectivity of nickel-catalyzed [3 + 2] cycloaddition of cyclopropenones and α,β-unsaturated ketones: A computational study

Lingling Liu, Hongli Wu, Genping Huang*

Department of Chemistry, School of Science and Tianjin Key Laboratory of Molecular Optoelectronic Sciences, Tianjin University, Tianjin 300072, China

ARTICLE INFO

Article history:
Received 25 February 2021
Received in revised form 31 March 2021
Accepted 1 April 2021
Available online 3 April 2021

Keywords:
Nickel catalyst
Cycloaddition
Mechanism
Selectivity
DFT calculations

ABSTRACT

Density functional theory calculations have been performed to investigate the nickel-catalyzed [3 + 2] cycloaddition of cyclopropenones and α,β-unsaturated ketones. The computations show that the overall catalytic cycle consists of four major steps, including: (1) C-C oxidative addition of the cyclopropenone to afford the four-membered nickelacycle, (2) isomerization, (3) migratory insertion *via* a 4,1-insertion fashion, and (4) C-C reductive elimination to deliver the [3 + 2] cycloaddition product. The enantioselectivity is mainly attributed to the π-π interaction between the diphenylcyclopropenone moiety and the phenyl substituent of the oxazoline ring of the ligand. The chemoselectivity of the C = O *versus* C = C insertion was rationalized in terms of the steric effect.

Transition metal-catalyzed cycloaddition reactions have gained tremendous research interest in organic synthesis, which provide one of the most powerful tools for the construction of carbo- and heterocycles [1–4]. In particular, the small ring systems (*i.e.*, cyclopropanes and cyclopropenes) have been widely employed in this type of transformation, due to that the relief of the ring strain would provide the driving force for the C-C oxidative addition to the metal center to afford the key metallacycles [2,3]. However, despite the significant progress has been witnessed, the development of the enantioselective reactions remains a central challenge in this field. In this context, Li and co-workers very recently reported an elegant example of the nickel-catalyzed [3 + 2] cycloaddition of α,β-unsaturated ketones/imines with cyclopropenones under relatively mild reaction conditions (Scheme 1) [4]. The salient feature of the reaction is the excellent enantioselectivity and exclusive chemoselectivity. It was found that with the combination of the pre-catalyst $Ni(cod)_2$ and the chiral quinoline-oxazoline ligand L, the reactions of cyclopropenones **1** and α,β-unsaturated ketones/imines **2** can give the [3 + 2] cycloaddition products *R*-**3** exclusively with excellent enantioselectivity (up to 98% *ee*), providing a highly efficient strategy for the enantioselective synthesis of the γ-alkenyl butenolides and γ-lactams [5].

The originally proposed reaction mechanism is depicted in Scheme 2. It was suggested that the reaction is initiated by the C—C oxidative addition of cyclopropenone **1** to give the four-membered nickelacycle **A**, from which the coordination of the incoming α,β-unsaturated ketone/imine **2** to the Ni center leads to intermediate **B**. This intermediate can undergo the selective migratory insertion of C=E into the Ni-C(acyl) bond to afford η^1-allyl Ni(II) intermediate **C-1** or η^3-allyl Ni(II) intermediate **C-2**. The catalytic cycle is then closed by the C—C reductive elimination to forge the [3 + 2] cycloaddition product. Alternatively, the migratory insertion of **2** into the Ni-C(acyl) bond can occur *via* a 4,1-insertion fashion to produce the eight-membered nickelacycle **C-3**, from which an η^1-η^3 allylic isomerization can take place to deliver **C-2**.

Considering the detailed reaction mechanism and the origins of the enantio- and chemoselectivities remain unclear, we therefore decided to investigate the title reaction computationally by means of density functional theory (DFT) calculations at the level of B3LYP-D3(BJ)-$SMD_{(toluene)}$/6−311+G(d,p)-SDD//B3LYP-D3(BJ)/6−31G(*d*)-LANL2DZ (see Supporting information for computational details) [6]. The experimentally used diphenylcyclopropenone **1a** and α,β-unsaturated ketone **2a** were selected as the model substrates (Fig. 1). To be noted, since that the redox-active quinoline-oxazoline ligand L was employed in the reaction, both singlet (closed- and open-shell) and triplet spin states of all species were considered, and the spin-crossover phenomenon was indeed observed [7]. For the sake of clarity, in the main text we will only present the most favorable pathway, and the other results are provided in Supporting information.

As shown in Fig. 1, intermediate $\mathbf{IM1}^{OSS}$, which is generated by the highly exergonic ligand exchange process between pre-catalyst $Ni(cod)_2$ and ligand L (see Supporting information for details), was chosen as the starting point of the calculations. The coordination of

* Corresponding author.
E-mail address: gphuang@tju.edu.cn (G. Huang).

https://doi.org/10.1016/j.cclet.2021.04.006

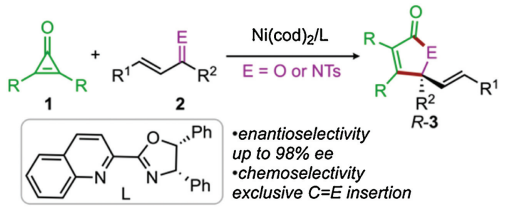

Scheme 1. Ni(0)-catalyzed [3 + 2] cycloaddition of cyclopropenones **1** and α,β-unsaturated ketones/imines **2**.

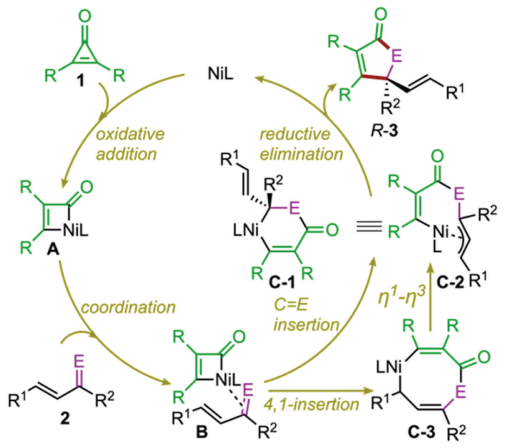

Scheme 2. Proposed reaction mechanism.

the C—C double bond of diphenylcyclopropenone **1a** to the Ni center of **IM1**^{OSS} leads to intermediate **IM2**^{CSS}, which was calculated to be exergonic by 2.8 kcal/mol. The computations show that although **IM2**^{triplet} is much less stable than **IM2**^{CSS} (see Supporting information for the minimum energy crossing point), the subsequent C—C oxidative addition was found to occur in the triplet state *via* transition state **TS1**^{triplet} rather than that in the singlet state (see Supporting information for details) [8], with an energy barrier of 8.8 kcal/mol relative to **IM2**^{triplet} (*i.e.*, 17.3 kcal/mol relative to **IM2**^{CSS}). The C—C oxidative addition was found to be exergonic, and the resulted intermediate four-membered nickelacycle **IM3**^{triplet} is more stable than **IM2**^{triplet} by 5.5 kcal/mol.

According to the proposed reaction mechanism (Scheme 2), the next step of the reaction is the migratory insertion of α,β-unsaturated ketone **2a** into the Ni-C bond. The reaction occurring directly from **IM3**^{triplet} was first considered. However, the energy barriers were computed to be relatively high (see the Supporting Information for details). Instead, an isomerization of **IM3**^{triplet} through the rotation of the Ni-C(alkenyl) bond *via* transition state **TS2**^{triplet} was found to take place, requiring an energy barrier of only 3.1 kcal/mol relative to **IM3**^{triplet}. The resulted nickelacycle **IM4**^{triplet}, differing in the relative orientation of Ni-C(alkenyl) bond, is slightly higher in energy than **IM3**^{triplet} by 1.6 kcal/mol.

Though the C—C oxidative addition and the isomerization were computed to occur preferentially at the triplet state, the ensuing reaction steps, *i.e.*, migratory insertion and C—C reductive elimination, were found to take place at the singlet state (see Supporting information for the minimum energy crossing point). Starting from the square planar **IM4**^{CSS}, which is much more stable than **IM4**^{triplet} by 10.5 kcal/mol, the possible pathways leading to final [3 + 2] cycloaddition products *R*-**3a** and *S*-**3a** were all considered. The computations show that the migratory insertion into the Ni-C(acyl) bond is much more favored than that into the Ni-C(alkenyl) bond (see Supporting information for details). Moreover, the 4,1-insertion, due to the presence of the additional stabilization of the C^3—C^4 double bond to the Ni center, was computed to be much more favored than the 2,1-insertion (*i.e.*, C=O insertion) [9,10].

The migratory insertion begins with the coordination of the C^3–C^4 double bond of **2a** to the Ni center of **IM4**^{CSS}. The resulted intermediates *R*-**IM5**^{CSS} and *S*-**IM5**^{CSS} then undergo the 4,1-insertion *via* transition states *R*-**TS3**^{OSS} and *S*-**TS3**^{OSS}, respectively.

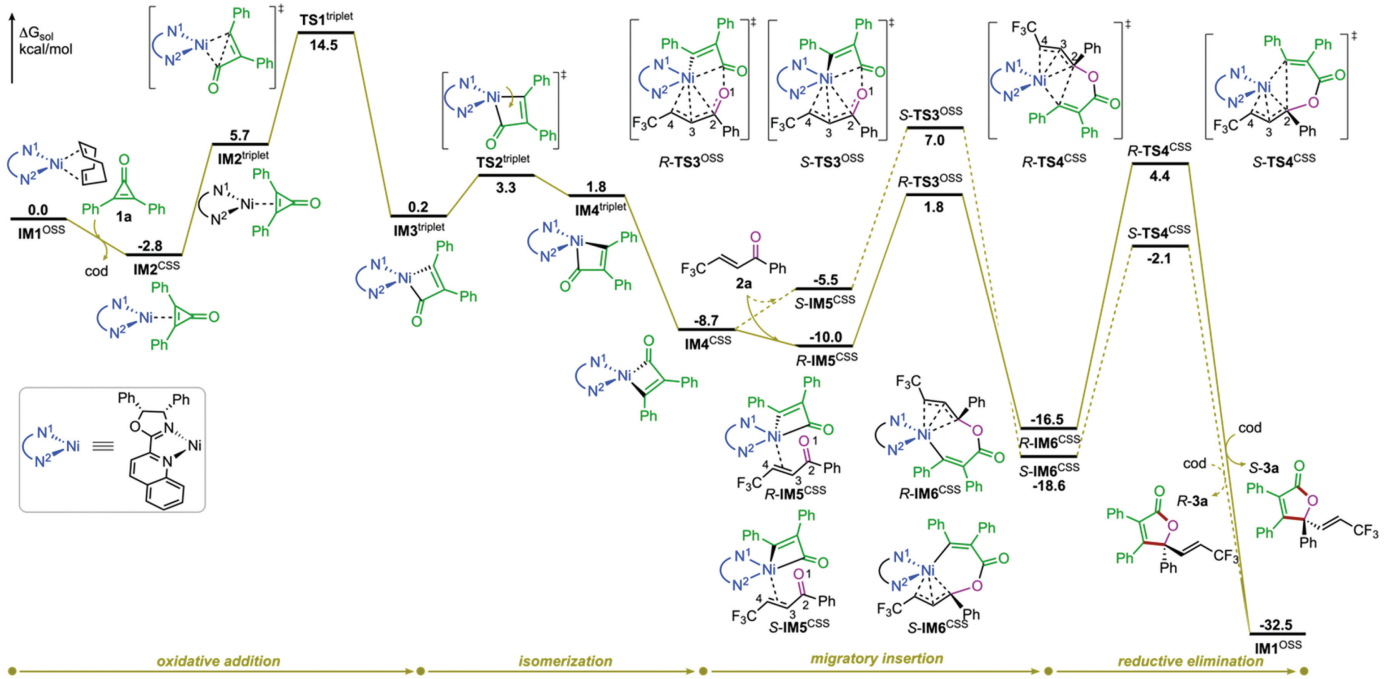

Fig. 1. Calculated energy profile of the Ni(0)-catalyzed [3 + 2] cycloaddition of diphenylcyclopropenone **1a** and α,β-unsaturated ketone **2a**. Spin states are indicated in superscript (CSS refers to closed–shell singlet and OSS refers to open–shell singlet).

Interestingly, the IRC calculations imply that instead of the eight-membered nickelacycles (*e.g.*, **C-3**, Scheme 2), the 4,1-insertion leads directly to the η^3-allyl Ni(II) intermediates *R*-**IM6**^{CSS} and *S*-**IM6**^{CSS}, from which the C-C^2 reductive elimination can occur readily *via* transition states *R*-**TS4**^{CSS} and *S*-**TS4**^{CSS}, delivering the final [3 + 2] cycloaddition products *R*-**3a** and *S*-**3a**, respectively. It should be mentioned here that the C-C^4 reductive elimination was also considered in the calculations, which could give the experimentally not observed [3 + 4] cycloaddition products. The results show that the energies of the C-C^4 reductive elimination are much higher than those of the C-C^2 reductive elimination, thereby ruling out this possibility (see Supporting information for details).

The computations reveal that from intermediate **IM4**^{CSS}, the C-C reductive elimination is the irreversible step for the *R*-pathway, while for the *S*-pathway the irreversible step is the 4,1-insertion. The enantioselectivity of the reaction is thus determined by the competition between transition states *R*-**TS4**^{CSS} and *S*-**TS3**^{OSS}. The calculated energy difference of 2.6 kcal/mol (4.4 kcal/mol of *R*-**TS4**^{CSS} *versus* 7.0 kcal/mol of *S*-**TS3**^{OSS}) corresponds to a calculated enantioselectivity of 98% *ee* at the reaction temperature (25 °C), being in excellent agreement with the experimentally observed 95% *ee* [4].

The origins of the enantioselectivity are mainly attributed to the significant preference of 4,1-insertion transition state *R*-**TS3**^{OSS} over *S*-**TS3**^{OSS} (1.8 kcal/mol of *R*-**TS3**^{OSS} *versus* 7.0 kcal/mol of *S*-**TS3**^{OSS}). The optimized geometries of the key transition states are given in Fig. 2a. The results show that for the 4,1-insertion, the key bond distances in both *R*-**TS3**^{OSS} and *S*-**TS3**^{OSS} are quite similar. However, in *R*-**TS3**^{OSS}, the diphenylcyclopropenone moiety was found to be rearranged to parallel with the phenyl substituent of the oxazoline ring of the ligand (highlighted in green, Fig. 2). As a consequence, the π-π interaction was observed in *R*-**TS3**^{OSS}, as evidenced by the reduced density gradient analysis of *R*-**TS3**^{OSS} (Fig. 2b). On the other hand, in *S*-**TS3**^{OSS}, no such interaction can be found due to the opposite orientation of the two moieties. Therefore, the presence of the additional π-π interaction makes *R*-**TS3**^{OSS} much lower in energy than *S*-**TS3**^{OSS}, leading to the experimentally observed enantioselectivity. This argument is also in accordance with the experiments that the absolute configuration of the product was found to be dictated by that of the 5-position in the ligand (*i.e.*, the configuration of the phenyl substituent of the oxazoline ring) [4]. The additional calculations using the ligand with the opposite configuration of the phenyl substituent of the oxazoline ring were further performed to support our argument. The results indeed show that the complementary enantioselectivity should be observed in the reaction (see Supporting information for details).

The trend of the reactivity of the C-C^2 reductive elimination was found to be opposite to that of the 4,1-insertion, and *R*-**TS4**^{CSS} was calculated to be much higher in energy than *S*-**TS4**^{CSS} by 6.5 kcal/mol (4.4 kcal/mol of *R*-**TS4**^{CSS} *versus* -2.1 kcal/mol of *S*-**TS4**^{CSS}). The origins of the reactivity difference are mainly due to that in *R*-**TS4**^{CSS}, the π-π interaction observed in *R*-**TS3**^{OSS} is absent in order to achieve the geometry of the C-C^2 reductive elimination. Instead, the steric repulsions between the diphenylcyclopropenone moiety and the phenyl substituents of the oxazoline ring were found (2.14 and 2.31 Å, Fig. 2a), thus enabling the opposite reactivity.

Finally, the chemoselectivity of the C=O *versus* C=C insertion was investigated. As shown in Fig. 3, the C=C insertion was found to proceed *via* the 1,4-insertion through the triplet transition state **TS5**^{triplet} with an energy barrier of 17.3 kcal/mol relative to *R*-**IM5**^{CSS}. The C=C insertion was calculated to be higher in energy than the C=O insertion (*via R*-**TS3**^{OSS}) by 5.5 kcal/mol, being in line with the experimentally observed exclusive C=O insertion [4]. Scrutiny of the optimized geometries of *R*-**TS3**^{OSS} and **TS5**^{triplet} (Figs. 2 and 3) shows that the origins of the chemoselectivity could be mainly due to the steric effect. It was found that the distance of the forming C-O^1 bond in *R*-**TS3**^{OSS} is 1.85 Å. However, in **TS5**^{triplet}, the distance of the forming C-C^4 bond is quite long, being 2.33 Å, which is probably due to the steric replusion between C^4 group and the acyl group is greater than that between the O^1 atom and the acyl group. Furthermore, the interactions between the Ni center and the allyl group in *R*-**TS3**^{OSS} is stronger than that in **TS5**^{triplet} (Ni-C^2 = 2.52, Ni-C^3 = 2.06 and Ni-C^4 = 2.02 Å in *R*-**TS3**^{OSS} *versus* Ni-

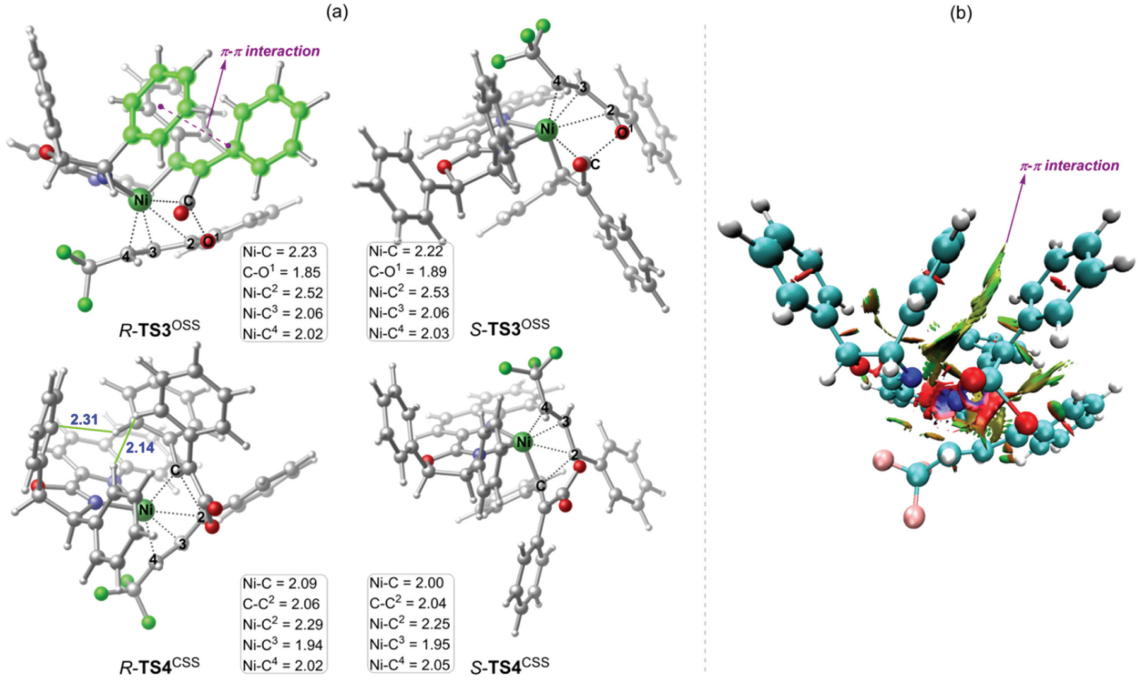

Fig. 2. (a) Optimized geometric structures of the key transition states. Bond distances are given in Å. (b) Reduced density gradient analysis of *R*-**TS3**^{OSS}.

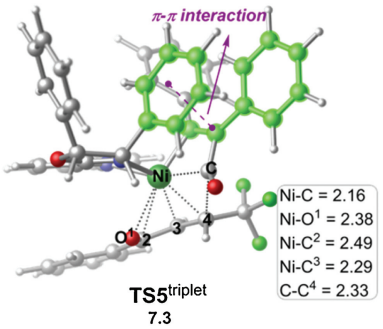

Fig. 3. C=C insertion *via* the 1,4-insertion. Bond distances and energy are given in Å and kcal/mol, respectively.

C^2 = 2.49, Ni-C^3 = 2.29 and Ni-O^1 = 2.38 Å in **TS5**^{triplet}). The combination of these two factors could result in the energy of *R*-**TS3**^{OSS} being much lower than **TS5**^{triplet}.

To summarize, we have herein presented a mechanistic study on the nickel-catalyzed [3 + 2] cycloaddition of cyclopropenones and α,β-unsaturated ketones by means of DFT calculations. The computations show that the reaction is initiated by the C-C oxidative addition of the cyclopropenone to afford the four-membered nickelacycle, from which an isomerization was required prior to the migratory insertion. The migratory insertion was found to proceed through a 4,1-insertion fashion to give the η^3-allyl Ni(II) intermediate. The catalytic cycle is then completed by the C-C reductive elimination to deliver the [3 + 2] cycloaddition product. The enantioselectivity of the reaction is determined by the competition between the C-C reductive elimination of the *R*-pathway and the 4,1-insertion of the *S*-pathway. The origins of the enantioselectivity are mainly attributed to the π-π interaction between the diphenylcyclopropenone moiety and the phenyl substituent of the oxazoline ring of the ligand. The experimentally observed exclusive C = O insertion was ascribed to the steric effect. The present results provide a number of new insights into the nickel-catalyzed cycloadditions involving small-ring systems, which should be helpful for the better understanding of related reactions and provide important implications for the future design of new catalytic systems.

Declaration of competing interest

The authors declare that they have no known competing financial interests or personal relationships that could have appeared to influence the work reported in this paper.

Acknowledgment

This work was supported by the National Natural Science Foundation of China (Nos. 22073066, 21503143 and 21975179).

Appendix A. Supplementary data

Supplementary material related to this article can be found, in the online version, at doi:https://doi.org/10.1016/j.cclet.2021.04.006.

References

[1] (a) R. Peng, Y. Xu, Q. Cao, Chin. Chem. Lett. 29 (2018) 1465–1474;
(b) L. Wang, Z. Yu, Chin. J. Org. Chem. 40 (2020) 3536–3558;
(c) A. Roglans, A. Pla-Quintana, M. Sola, Chem. Rev. 121 (2021) 1894–1979;
(d) J. Wang, S.A. Blaszczyk, X. Li, et al., Chem. Rev. 121 (2021) 110–139.
[2] (a) P. Chen, B.A. Billett, T. Tsukamoto, et al., ACS Catal. 7 (2017) 1340–1360;
(b) R. Vicente, Chem. Rev. 121 (2021) 162–226;
(c) M. Murakami, N. Ishida, Chem. Rev. 121 (2021) 264–299.
[3] (a) M. Murakami, S. Ashida, T. Matsuda, J. Am. Chem. Soc. 127 (2005) 6932–6933;
(b) A. Schuster-Haberhauer, R. Gleiter, O. Körner, Organometallics 27 (2008) 1361–1366;
(c) P. Chen, T. Xu, G. Dong, Angew. Chem. Int. Ed. 53 (2014) 1674–1678;
(d) P. Chen, J. Sieber, C.H. Senanayake, et al., Chem. Sci. 6 (2015) 5440–5445;
(e) T. Kondo, Y. Kaneko, Y. Taguchi, et al., J. Am. Chem. Soc. 124 (2002) 6824–6825;
(f) T. Lin, C. Zhu, P. Zhang, et al., Angew. Chem. Int. Ed. 55 (2016) 10844–10848;
(g) Q. Li, G. Jiang, L. Jiao, et al., Org. Lett. 12 (2010) 1332–1335.
[4] D. Bai, Y. Yu, H. Guo, et al., Angew. Chem. Int. Ed. 59 (2020) 2740–2744.
[5] (a) B. Mao, M. Fañanas-Mastral, B.L. Feringa, Chem. Rev. 117 (2017) 10502–10566;
(b) S. Wang, Y. Liu, N. Cramer, Angew. Chem. Int. Ed. 58 (2019) 18136–18140;
(c) J. Ji, L. Lin, Q. Tang, et al., ACS Catal. 7 (2017) 3763–3767;
(d) G.L. Hamilton, E.J. Kang, M. Mba, et al., Science 317 (2007) 496–499.
[6] (a) Y. Li, Z. Lin, Organometallics 32 (2013) 3003–3011;
(b) X. Hong, D. Holte, D.C.G. Götz, et al., J. Org. Chem. 79 (2014) 12177–12184;
(c) Y. Liu, Y. Tang, Y. Jiang, et al., ACS Catal. 7 (2017) 1886–1896;
(d) S. Yang, Y. Xu, J. Li, Org. Lett. 18 (2016) 6244–6247;
(e) Y. Luo, C. Shan, Song Liu, et al., ACS Catal. 9 (2019) 10876–10886;
(f) I. Nohira, S. Liu, R. Bai, et al., J. Am. Chem. Soc. 142 (2020) 17306–17311;
(g) Y. Li, Y. Luo, L. Peng, et al., Nat. Commun. 11 (2020) 1–13.
[7] (a) Z. Zhang, J. Zhang, F.K. Sheong, et al., ACS Catal. 10 (2020) 12454–12465;
(b) J. Guo, H. Wang, S. Xing, et al., Chem 5 (2019) 1–15;
(c) M. Yuan, Z. Song, S.O. Badir, et al., J. Am. Chem. Soc. 142 (2020) 7225–7234;
(d) L. Hu, H. Chen, J. Am. Chem. Soc. 139 (2017) 15564–15567;
(e) Y. Yu, G. Luo, J. Yang, Catal. Sci. Technol. 9 (2019) 1879–1890;
(f) L. Lin, C. Daia, J. Zhu, Org. Chem. Front. 8 (2021) 1531–1543;
(g) S. Li, Y. Lan, Chem. Commun. 56 (2020) 6609–6619.
[8] Y. Luo, C. Shan, S. Liu, ACS Catal. 9 (2019) 10876–10886.
[9] H. Zou, Z. Wang, G. Huang, Chem. Eur. J. 23 (2017) 12593–12603.
[10] (a) L. Xu, Q. Zhu, G. Huang, B. Cheng, Y. Xia, J. Org. Chem. 77 (2012) 3017–3024;
(b) W. Guo, Y. Xia, J. Org, Chem. 80 (2015) 8113–8121;
(c) W. Guo, T. Zhou, Y. Xia, Organometallics 34 (2015) 3012–3020;
(d) L. Xu, X. Zhang, M.S. McCammant, et al., J. Org. Chem. 81 (2016) 7604–7611;
(e) Y. Liu, Y. Tang, Y.Y. Jiang, et al., ACS Catal. 7 (2017) 1886–1896;
(f) G. Lu, R.Y. Liu, Y. Yang, et al., J. Am. Chem. Soc. 139 (2017) 16548–16555;
(g) X. Lv, F. Huang, Y.B. Wu, G. Lu, Catal. Sci. Technol. 8 (2018) 2835–2840;
(h) X.W. Chen, L. Zhu, Y.Y. Gui, et al., J. Am. Chem. Soc. 141 (2019) 18825–18835;
(i) X. Li, X. Ren, H. Wu, et al., Chin. Chem. Lett. 32 (2021) 9–12;
(j) H. Zou, Z.L. Wang, Y. Cao, G. Huang, Chin. Chem. Lett. 29 (2018) 1355–1358;
(k) X. Li, H. Wu, Z. Wu, G. Huang, J. Org. Chem. 84 (2019) 5514–5523;
(l) G. Huang, P. Liu, ACS Catal. 6 (2016) 809–820;
(m) M. Zhang, G. Huang, Dalton Trans. 45 (2016) 3552–3557;
(n) L. Hu, Z. Wu, G. Huang, Org. Lett. 20 (2018) 5410–5413.